Organic/inorganic hybrid synaptic transistors gated by proton conducting methylcellulose films

Chang Jin Wan,[1,2] Li Qiang Zhu,[2] Xiang Wan,[1] Yi Shi,[1,a)] and Qing Wan[1,2,a)]
[1]*School of Electronic Science & Engineering, and Collaborative Innovation Center of Advanced Microstructures, Nanjing University, Nanjing 210093, China*
[2]*Ningbo Institute of Material Technology and Engineering, Chinese Academy of Sciences, Ningbo 315201, China*

(Received 21 September 2015; accepted 20 January 2016; published online 29 January 2016)

The idea of building a brain-inspired cognitive system has been around for several decades. Recently, electric-double-layer transistors gated by ion conducting electrolytes were reported as the promising candidates for synaptic electronics and neuromorphic system. In this letter, indium-zinc-oxide transistors gated by proton conducting methylcellulose electrolyte films were experimentally demonstrated with synaptic plasticity including paired-pulse facilitation and spatiotemporal-correlated dynamic logic. More importantly, a model based on proton-related electric-double-layer modulation and stretched-exponential decay function was proposed, and the theoretical results are in good agreement with the experimentally measured synaptic behaviors. © *2016 AIP Publishing LLC*.
[http://dx.doi.org/10.1063/1.4941080]

Conventional computers based on CMOS technology and von Neumann architecture excel in logic and accurate scientific calculations, but it cannot compete with biological brains where the problems involve interaction with the real world and where both the inputs and outputs are often imprecisely specified.[1] Inspired by the energy-efficient and cognitive ability of a biological brain, neuromorphic computing has emerged as an attractive computation paradigm that complements the von Neumann architecture.[2,3] In order to realize neuromorphic computing, software- and hardware-based approaches have been proposed. However, the software-based approaches are faced with significant challenges in energy dissipation since the algorithm is essentially run by conventional von Neumann computers with limited parallelism.[4] The hardware-based approaches can potentially overcome such challenges by implementing massive parallelism at a physical level. Synaptic electronics have aroused wide attention in recent years, which aim at developing artificial synaptic devices to emulate the memory and computation performed by biological synapses. Up until now, a broad spectrum of synaptic devices has been developed with essential synaptic functions.[4–11] Emerging memory structures have several characteristics such as historical-dependent analogue-like state, which are suitable for neuromorphic systems. For example, amorphous InGaZnO memristor was proposed to mimic an experimentally observed form of Hebbian learning rule known as spike-timing-dependent plasticity (STDP), which is mainly due to oxygen ion migration/diffusion induced conductance changes.[11]

Carriers in semiconductor channel layers can be strongly accumulated or depleted by electrolyte gating due to the extremely large electric-double-layer (EDL) capacitance formed at the electrolyte/semiconductor interface.[12–14] The EDL can be regarded as a nanoscale capacitor with a huge specific capacitance above 1.0 μF/cm^2. Recently, three-terminal EDL transistors gated by ion conducting electrolytes were also proposed as the promising candidates for synaptic electronics.[15–19] In previous reports, the gate pulse and channel current (or channel conductance) were defined as the synaptic stimulus and synaptic weight, respectively. The synaptic weight of the transistors can thus be modified by tuning the pattern and timing of the stimuli, which enable the plasticity behaviors as a biological synapse. However, a physical insight into such synaptic devices is still lacking.

Indium zinc oxide (IZO) film with high mobility (10–50 cm^2/Vs) and large-area uniformity can be deposited by radio-frequency sputtering at a low temperature or even at a room temperature.[20] Thin-film transistors with IZO channel layers are very good candidates for switching or driving transistors in the next generation and/or flexible flat panel displays, sensors, and other new-concept applications, such as neuromorphic systems.[21,22] In this letter, IZO-based EDL transistors gated by proton conducting methylcellulose electrolyte films were fabricated and used for synaptic function emulation. Synaptic plasticity emulations were also theoretically modeled based on the proton-related EDL modulation and stretched-exponential decay function, and the theoretical results were in good agreement with the experimental results. These findings could provide a useful guideline for designing artificial synapses for neuromorphic computing systems.

Methylcellulose (MC) is a chemical compound derived from cellulose, which has good thermal, chemical, mechanical stabilities. It is synthetically produced by a substitution reaction that the hydroxyl residues (-OH functional groups) are replaced by methoxide (-OCH_3 groups). These functional groups enable the MC film to absorb water molecules, which contributes to the high proton conductivity.[23] MC film with a good stability and a high proton conductivity is of great interest for EDL transistors' fabrication and synaptic electronics application. First, MC powder (Sinopharm Chemical Reagent Co., Ltd.) was mixed into deionized water at 85 °C for 5 min and then cooled in air ambient to obtain a homogeneous solution with a concentration of 1.0 wt. %. Then, the solution was spin-coated onto the ITO glass substrate and dried in air ambient at 50 °C for 2 h. The thickness (D) of the MC film is estimated to be ~9.0 μm. After that, 150-nm-thick IZO patterns

a)Electronic addresses: wanqing@nju.edu.cn and yshi@nju.edu.cn

(1000 μm × 150 μm) were deposited on the MC film by magnetron sputtering at room temperature with the use of a nickel shadow mask. As shown in Fig. 2(a), when the gap between the shadow mask and the substrate is about 50 μm, a thin IZO channel layer with the thinnest part of ~30 nm can be self-assembled between the IZO source/drain electrodes due to the reflection of IZO nanoparticles at the mask edge and dimensional extension by IZO nanoparticles with a low incident angle.[17,24] Proton conductivity and specific capacitance of the MC films were measured by a Solartron 1260A impedance analyzer. The electrical performances of the IZO synaptic transistors were characterized by using a Keithley 4200 SCS semiconductor parameter characterization system.

The proton conductivity of the MC film is determined from the Cole-Cole plot, as shown in Fig. 1(a). Proton conductivity (σ) is calculated by a relation $\sigma = D/(R - R_0)A$, where D, R, R_0, and A are the thickness of MC film, the intersecting point on the real axis of Cole-Cole plots, the resistance of the electrodes, and the resistance of the electrode area, respectively.[25,26] Here, A is 1.5×10^{-3} cm^2, and R_0 is ~30 Ω. Therefore, the σ value is estimated to be $\sim 6.5 \times 10^{-4}$ S/cm. Figure 1(b) shows the frequency dependent specific capacitance of the proton conducting MC film measured with an in-plane test structure (inset in Fig. 1(b)). The specific capacitance increases with decreasing frequency and gradually reaches the maximum value (C_{DL}) of ~3.1 μF/cm^2 at 1.0 Hz, which indicates the formation of EDL at the electrode/electrolyte interface.[13]

Figure 2(a) shows the schematic image of IZO-based synaptic transistor gated by MC film on the glass substrate with two in-plane gates. The voltage applied on the in-plane gates can be capacitively coupled to the IZO channel.[24] Figure 2(b) shows the transfer curve of the IZO-based synaptic transistor with a constant V_{DS} of 1.5 V. The gate voltage was swept from −1.0 V to 0.8 V and then back. A clear anticlockwise hysteresis window of ~0.25 V was observed, which is likely due to the mobile protons within the MC electrolyte film.[13] The subthreshold swing (SS), current on/off ratio (I_{on}/I_{off}), and the threshold voltage (V_{TH}) are estimated to be ~85 mV/decade, $\sim 2.5 \times 10^6$, and ~0.14 V, respectively. In addition, the field-effect electron mobility (μ_{FE}) at the saturation region ($V_{DS} > V_{GS} - V_{TH}$) is estimated to be ~21.2 cm^2/V.s by the following equation:

$$I_{DS} = \frac{WC_{DL}\mu_{FE}}{2L}(V_{GS}-V_{TH})^2, \quad (1)$$

where W, L, and C_{DL} are the channel width, channel length, and specific capacitance of the EDL, respectively.

Excitatory postsynaptic currents (EPSCs) or inhibitory PSCs (IPSCs) can be triggered by the potential spikes from the presynaptic neurons, which are collectively processed by the postsynaptic neurons to establish spatial and temporal correlated functions.[27] As previously reported, the gate pulse and channel current (or channel conductance) were defined

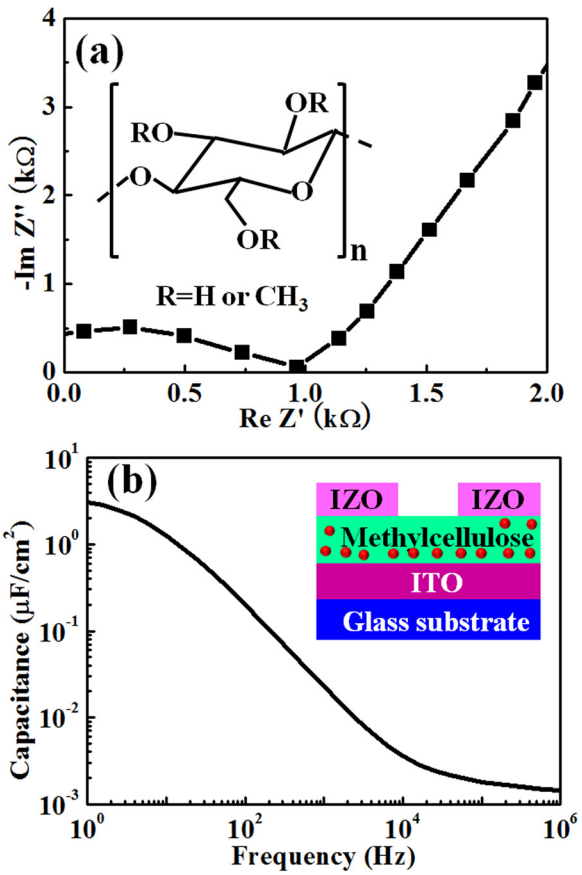

FIG. 1. (a) The proton conducting characteristics of the methylcellulose electrolyte film: Cole-cole plot. Inset: the molecular formula of methylcellulose. (b) The frequency dependent specific capacitance of the methylcellulose electrolyte film. Inset: the capacitance test structure with two in-plane IZO electrodes.

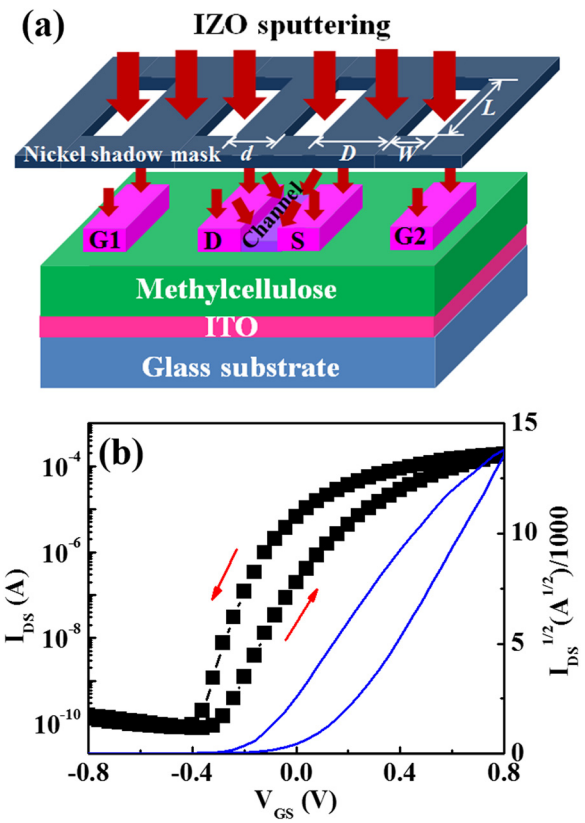

FIG. 2. (a) Schematic image of the fabrication of IZO-based synaptic transistor gated by methylcellulose electrolyte film by a nickel shadow mask self-assembling method. (b) Transfer characteristics of the IZO-based synaptic transistor operated at $V_{DS} = 1.5$ V. The square root of I_{DS} vs V_{GS} is plotted as the blue line.

as the synaptic stimulus and synaptic weight, respectively. The synaptic weight of the devices can be modified by tuning the pattern and timing of the stimuli, which is similar to that in a biological synapse. In our experiment, presynaptic spikes were applied on the gate electrodes in order to emulate the synaptic behaviors. The channel current measured at $V_{DS} = 0.1$ V was regarded as EPSC. Figure 3(a) shows the EPSC response triggered by a presynaptic spike (40 ms, 0.1 V) applied on Gate1 (G1). The inset of Fig. 3(a) shows the schematic diagram for EPSC measurement. As shown in Fig. 3(b), during a presynaptic spike, protons are electrically triggered and migrated to the IZO channel/methylcellulose electrolyte interface. The transient accumulation of protons then induces a sharp increase in the channel current by the strong EDL electrostatic coupling. When the spike ends, protons will diffuse back to the equilibrium positions due to the concentration gradient.[28] The decay of proton concentration at the IZO/methylcellulose interface thus results in a gradual decay of the channel current.

As mentioned above, the increment of the channel current is due to the accumulation of protons at the MC/IZO interface. We assumed that there is no interfacial electrochemical reaction at a low gate voltage ($V_{GS} \leq 1.5$ V).[13,29] Thus, the electrolyte film can be simply modeled as a resistor-capacitor (RC) circuit, as shown in Fig. 3(b). The voltage across the electrolyte film yields

$$V_{DL}(t) = V_A \cdot \left[1 - \exp\left(-\frac{t}{\tau_{DL}}\right)\right], \tag{2}$$

where V_A and τ_{DL} are the applied voltage and time constant of the RC circuit, respectively. During the charging process, the induced carriers in the IZO channel layer will increase the channel conductance. If the duration of a positive spike is T, the proton concentration ($t \leq T$) will increase with the charging voltage. According to Eq. (2), the proton concentration ($\Delta N(t)_{t \leq T}$) can be written by the following equation:

$$\Delta N(t)_{t \leq T} = C_{DL}(V_{GS} - V_{TH})\left[1 - \exp\left(-\frac{t}{\tau_{DL}}\right)\right] \Big/ ZqWL\delta_E, \tag{3}$$

where Z, q, and δ_E are the ionic valence ($Z = 1$ for proton), elementary charge, and the depth of the ion-accumulation layer in electrolyte, respectively. When the spike ends, protons will diffuse back to the equilibrium position gradually. Stretched-exponential decay has been widely applied for modeling relaxation process such as hydrogen diffusion in α-Si:H, oxygen vacancies' diffusion in the WO_x, etc.[30–33] In our case, the stretched-exponential function can also be used for modeling the proton relaxation processes in the proton conducting MC film. Thus, the proton concentration after the presynaptic spike ($t > T$) can be determined by the following equation:

$$\Delta N(t)_{t>T} = \Delta N(T)_{t \leq T} \cdot \exp\left[-\left(\frac{t-T}{\tau}\right)^{\beta}\right], \tag{4}$$

where τ and β are the time constant of ion relaxation and the stretch index ranged between 0 and 1, respectively. It should be noted here that the total EPSC (I_{DS}) can be determined by the relation: $I_{DS} = I_0 + \Delta I_{DS}$, where I_0 is the base channel current when no presynaptic spike is triggered ($V_{GS} = 0$ V), and ΔI_{DS} is the changes in the channel current (EPSC) induced by a presynaptic spike. The changes in conductivity ($\Delta\sigma$) of the semiconductor layer could be determined by the following relations:[34,35]

$$\Delta\sigma = \frac{\Delta J}{E} = \frac{\Delta I_{DS} L}{V_{DS} W \delta_S} \tag{5}$$

and

$$\Delta\sigma = \Delta n q \mu, \tag{6}$$

where ΔJ, E, δ_S, and Δn are the changes in current density, the electric-field intensity, the depth of the carrier-accumulation layer in the semiconductor, and the induced electron concentration, respectively. Therefore, ΔI_{DS} can be written as

$$\Delta I_{DS} = \frac{\Delta n q \mu \cdot V_{DS} W \delta_S}{L}. \tag{7}$$

Due to the huge EDL capacitance, the induced electron concentration should be approximately equal to the induced proton concentration ($\Delta n = \Delta N$). Thus, the EPSC amplitude (A(t)) can be deduced by substituting $\Delta N(t)_{t \leq T}$ and $\Delta N(t)_{t>T}$ into Eq. (7)

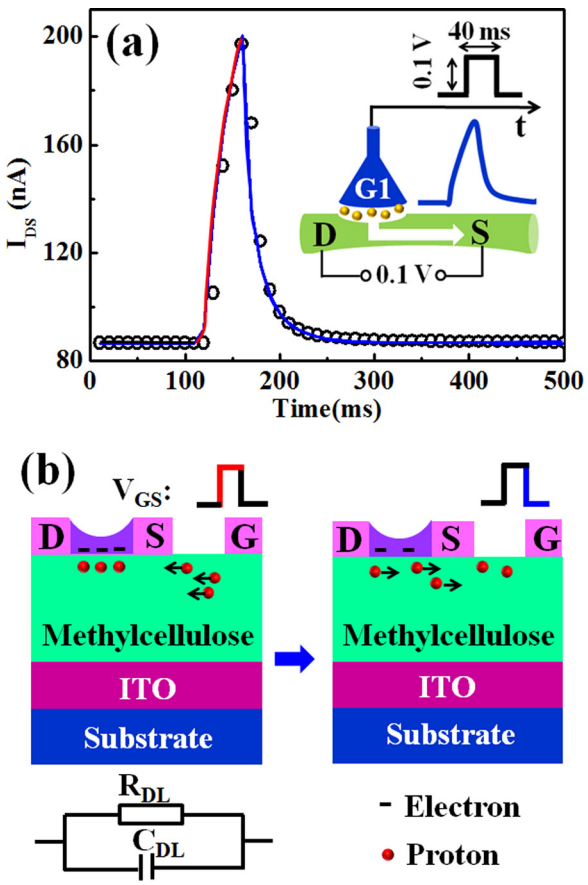

FIG. 3. (a) A typical EPSC response triggered by a presynaptic spike (40 ms, 0.1 V) applied on the in-plane gate electrode. The experimental data are plotted as open circles. The fitting curve is plotted as a solid line. Inset: the schematic illustration of the measurements of EPSC. (b) Schematic diagram illustrating the dynamic processes of an EPSC event. The EDL can be equivalent to a resistor-capacitor (RC) circuit with a resistor (R_{DL}) and a capacitor (C_{DL}) connected in parallel.

$$A(t) = \Delta I_{DS} = \begin{cases} \kappa \cdot \left[1 - \exp\left(-\frac{t}{\tau_{DL}}\right)\right] & t \le T \\ \kappa \cdot \left[1 - \exp\left(-\frac{T}{\tau_{DL}}\right)\right] \cdot \exp\left[-\left(\frac{t-T}{\tau}\right)^{\beta}\right] & t > T, \end{cases} \quad (8)$$

where $\kappa = \frac{C_{DL}\mu\delta_S \cdot V_{DS}(V_{GS}-V_{TH})}{ZL^2\delta_E}$. κ can be regarded as the EPSC amplitude triggered by a continuous presynaptic spike ($T \to \infty$). The measured EPSC is plotted as open circles in Fig. 3(a). The fitted result based on Eq. (8) is plotted as a solid line in Fig. 3(a). The fitting parameters of κ, τ_{DL}, τ, and β are estimated to be 766 nA, 257 ms, 9.0 ms, and 0.74, respectively. The fitting curve approaches the experimental results very well, indicating the validity of our proposed model.

Paired-pulse facilitation (PPF) is a short-term form of synaptic plasticity, which represents an amplitude increase in the second synaptic response when it follows shortly after the first one.[36,37] Figure 4(a) shows the EPSC response triggered by the two successive presynaptic spikes (0.1 V, 10 ms) with a time interval (ΔT) of 40 ms. The second EPSC peak (A_2) is ~156 nA, which is larger than the first EPSC peak (A_1) of ~148 nA. The inset in Fig. 4(a) schematically illustrates the measurements for PPF emulation. The facilitation ratios (A_2/A_1) are plotted as a function of ΔT, as shown in Fig. 4(b). The obtained PPF emulation results are in good agreement with that observed in biological systems.[36–38] According to Eq. (8), the EPSC triggered by the first spike would reach its maximum value (A_1) of $\kappa \cdot [1 - \exp(-\frac{T}{\tau_{DL}})]$ at the end of the spike ($t = T$). After that, the protons will diffuse back to their equilibrium positions yielding the stretched exponential function. During the second pulse, the residual protons triggered by the first spike will be added to the total proton concentration, which would induce an increment in EPSC as a result. Therefore, the amplitude of the second EPSC peak can be estimated by the following relation:

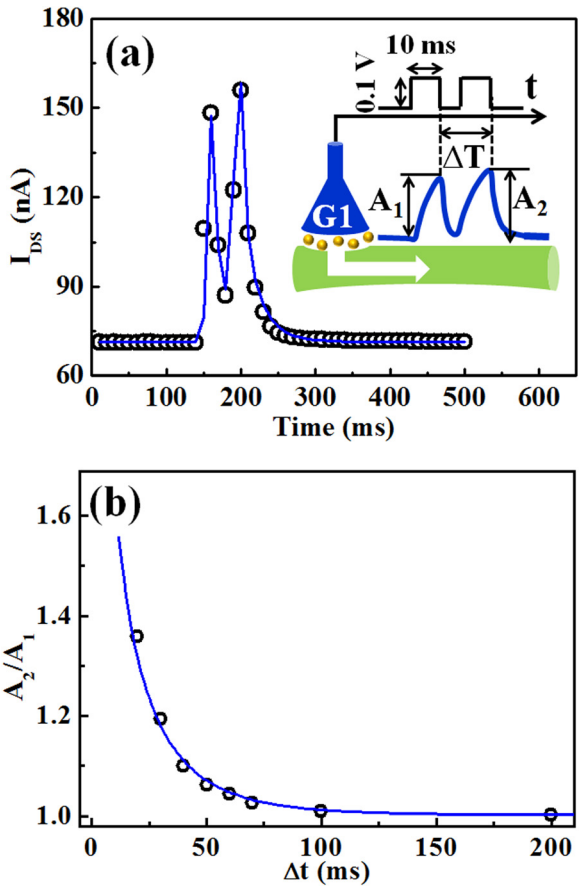

FIG. 4. (a) EPSCs triggered by two successive presynaptic spikes (0.1 V, 10 ms) with a time interval (ΔT) of 40 ms. The black open circles are the experimental data, and the blue solid line is the fitting curve. Inset: the schematic diagram for measuring PPF. (b) The facilitation ratios (A_2/A_1) are plotted as a function of ΔT. The black open circles are the experimental data, and the blue solid line is the fitting curve.

$$A_2 = \kappa \cdot \left[1 - \exp\left(-\frac{T}{\tau_{DL}}\right)\right] + \lambda \cdot \kappa \cdot \left[1 - \exp\left(-\frac{T}{\tau_{DL}}\right)\right] \times \exp\left[-\left(\frac{\Delta T}{\tau}\right)^{\beta}\right], \quad (9)$$

where λ is a factor related to the effective residual proton concentration contributed to the second EPSC. Then, the facilitation ratio (A_2/A_1) between the two EPSC amplitudes can be determined by the following equation:

$$F(\Delta T) = \frac{A_2}{A_1} = 1 + \lambda \cdot \exp\left[-\left(\frac{\Delta T}{\tau}\right)^{\beta}\right]. \quad (10)$$

The facilitation ratio (A_2/A_1) is plotted as a function of ΔT in Fig. 4(b). The blue solid line is the fitted by Eq. (10) with $\lambda = 2.2$. We find that the fitting curve approaches the experimental results very well.

Dynamic logics established by the spatiotemporal correlated spikes are also demonstrated in the proposed synaptic transistor with two in-plane gates (G1 and G2) as presynaptic terminals. Figure 5(a) shows the schematic diagram of such an emulation. Two presynaptic spikes P1 and P2 (0.1 V, 10 ms) with a time interval (ΔT) are applied on two presynaptic terminals G1 and G2, respectively. The zero time ($t = 0$) is defined as the time when P2 ends. The EPSC amplitudes measured at $t = 0$ are plotted as a function of ΔT, as shown in Fig. 5(b), which decrease asymmetrically with increasing $|\Delta T|$. The EPSC amplitudes decrease gradually from 520 nA to 217 nA when ΔT changes from 0 to −150 ms, while no significant change in the EPSC amplitudes can be observed when $\Delta T > 0$.

When $\Delta T > 0$, i.e., the spike P1 triggers after spike P2, the EPSC amplitude measured at $t = 0$ is equal to the EPSC individually triggered by P2. When $\Delta T < 0$, i.e., the spike P1 triggers before spike P2, the EPSC amplitude measured at $t = 0$ is the summed current of EPSC1 triggered by P1 and EPSC2 triggered by P2. Therefore, the summed current can be written as $\lambda' A_1 \cdot \exp[-(\frac{-\Delta T}{\tau})^{\beta}] + A_2$, where λ' is a factor related to the effective residual proton concentration (triggered by P1) contributed to the summed current, and $A_1 = \kappa_1 \cdot [1 - \exp(-\frac{T}{\tau_{DL}})]$ and $A_2 = \kappa_2 \cdot [1 - \exp(-\frac{T}{\tau_{DL}})]$ are the EPSC amplitudes individually triggered by P1 and P2, respectively. In conclusion, the EPSC amplitude at $t = 0$ can be determined by the following equation:

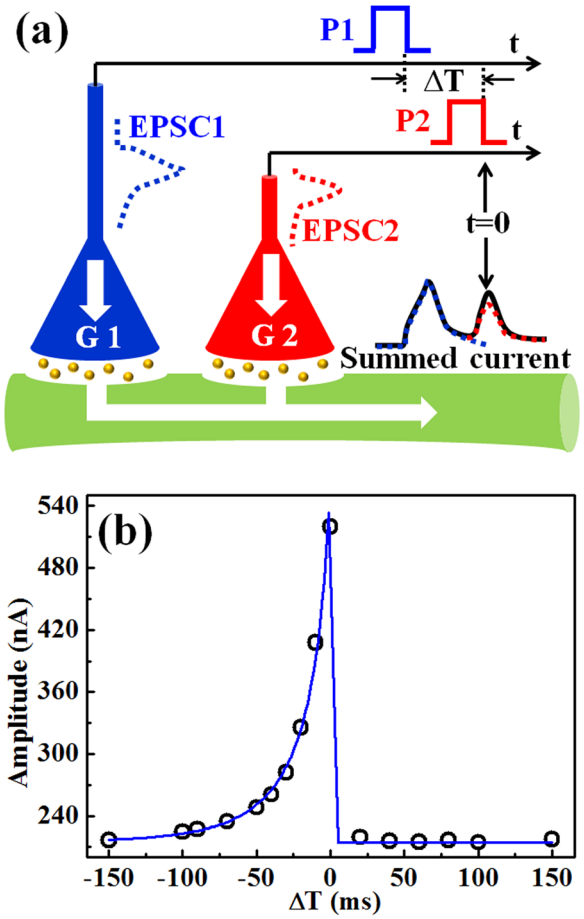

FIG. 5. (a) Schematic diagram of the measurement for dynamic logic established by spatiotemporal correlated spikes. (b) The EPSC amplitude measured at t = 0 is plotted as a function of time interval (ΔT). The experimental results are plotted as black open circles, and the blue solid line is the fitting curve.

$$A(\Delta T)_{t=0} = \begin{cases} \lambda' A_1 \cdot \exp\left[-\left(\dfrac{-\Delta T}{\tau}\right)^{\beta}\right] + A_2 & \Delta T \le 0 \\ A_2 & \Delta T > 0. \end{cases} \tag{11}$$

The EPSC amplitudes measured at t = 0 are plotted as a function of time interval (ΔT) in Fig. 5(b). Furthermore, the measured EPSC amplitudes are fitted by Eq. (11) and plotted as blue solid line in Fig. 5(b). λ', A_1, and A_2 are estimated to 0.92, 332 nA, and 217 nA, respectively. Again, we find that the fitting curve approaches the experimental results very well, indicating the validity of the proposed model.

In summary, synaptic plasticity including PPF and spatiotemporal-correlated dynamic logic were experimentally demonstrated in an organic/inorganic hybrid artificial synapse based on an IZO-based EDL transistor gated by methylcellulose electrolyte film. A model based on proton-related electric-double-layer modulation and stretched-exponential decay function was proposed, and the theoretical simulation results are consistent with the measured synaptic behaviors. Our results may provide an interesting guideline for artificial synapses and brain-inspired neuromorphic systems.

This work was supported by the National Science Foundation for Distinguished Young Scholars of China (No. 61425020), the National Natural Science Foundation of China (Nos. 11174300 and 11474293), and the Zhejiang Provincial Natural Science Foundation of China (No. LR13F040001).

[1]D. Kuzum, S. Yu, and H.-S. P. Wong, Nanotechnology **24**, 382001 (2013).
[2]S. Furber, IEEE Spectr. **49**, 44 (2012).
[3]C. K. Machens, Science **338**, 1156 (2012).
[4]S. M. Yu, B. Gao, Z. Fang, H. Y. Yu, J. F. Kang, and H.-S. P. Wong, Adv. Mater. **25**, 1774 (2013).
[5]T. Ohno, T. Hasegawa, T. Tsuruoka, K. Terabe, J. K. Gimzewski, and M. Aono, Nat. Mater. **10**, 591 (2011).
[6]F. Alibart, S. Pleutin, O. Bichler, G. Christian, S. G. Teresa, L. B. Bernabe, and D. A. Vuillaume, Adv. Funct. Mater. **22**, 609 (2012).
[7]C. Du, W. Ma, T. Chang, P. Sheridan, and W. D. Lu, Adv. Funct. Mater. **25**, 4290 (2015).
[8]T. Chang, S. H. Jo, and W. Lu, ACS Nano **5**, 7669 (2011).
[9]D. Kuzum, R. G. D. Jeyasingh, B. Lee, and H.-S. P. Wong, Nano Lett. **12**, 2179 (2012).
[10]R. Yang, K. Terabe, G. Q. Liu, T. Tsuruoka, T. Hasegawa, J. K. Gimzewski, and M. Aono, ACS Nano **6**, 9515 (2012).
[11]Z. Q. Wang, H. Y. Xu, X. H. Li, H. Yu, Y. C. Liu, and X. J. Zhu, Adv. Funct. Mater. **22**, 2759 (2012).
[12]A. S. Dhoot, J. D. Yuen, M. Heeney, I. McCulloch, D. Moses, and A. J. Heeger, Proc. Natl. Acad. Sci. U.S.A. **103**, 11834 (2006).
[13]H. T. Yuan, H. Shimotani, J. T. Ye, S. Yoon, H. Aliah, A. Tsukazaki, M. Kawasaki, and Y. Iwasa, J. Am. Chem. Soc. **132**, 18402 (2010).
[14]J. T. Ye, S. Inoue, K. Kobayashi, Y. Kasahara, H. T. Yuan, H. Shimotani, and Y. Iwasa, Nat. Mater. **9**, 125 (2010).
[15]Q. X. Lai, L. Zhang, Z. Y. Li, W. F. Stickle, R. S. Williams, and Y. Chen, Adv. Mater. **22**, 2448 (2010).
[16]K. Kim, C. L. Chen, Q. Truong, A. M. Shen, and Y. Chen, Adv. Mater. **25**, 1693 (2013).
[17]L. Q. Zhu, C. J. Wan, L. Q. Guo, Y. Shi, and Q. Wan, Nat. Commun. **5**, 3158 (2014).
[18]C. J. Wan, L. Q. Zhu, J. M. Zhou, Y. Shi, and Q. Wan, Nanoscale **5**, 10194 (2013).
[19]J. Shi, S. D. Ha, Y. Zhou, F. Schoofs, and S. Ramanathan, Nat. Commun. **4**, 2676 (2013).
[20]Y. Song, R. Xu, J. He, S. Siontas, A. Zaslavsky, and D. C. Paine, IEEE Electron Device Lett. **35**, 1251 (2014).
[21]H. Xu, L. F. Lan, M. Xu, J. H. Zou, L. Wang, D. Wang, and J. B. Peng, Appl. Phys. Lett. **99**, 253501 (2011).
[22]L. Q. Guo, Q. Wan, C. J. Wan, L. Q. Zhu, and Y. Shi, IEEE Electron Device Lett. **34**, 1581 (2013).
[23]A. S. Samsudin, W. M. Khairul, and M. I. N. Isa, J. Non-Cryst. Solids **358**, 1104–1112 (2012).
[24]J. Jiang, J. Sun, L. Q. Zhu, G. D. Wu, and Q. Wan, Appl. Phys. Lett. **99**, 113504 (2011).
[25]L. Q. Zhu, J. Sun, G. D. Wu, H. L. Zhang, and Q. Wan, Nanoscale **5**, 1980 (2013).
[26]Y. G. Jin, S. Z. Qiao, J. C. da Costa, B. J. Wood, B. P. Ladewig, and G. Q. Lu, Adv. Funct. Mater. **17**, 3304 (2007).
[27]G. Q. Bi and M. M. Poo, Nature **401**, 792 (1999).
[28]N. Liu, L. Q. Zhu, H. Xiao, C. J. Wan, Y. H. Liu, and J. Y. Chao, ACS Appl. Mater. Interfaces **7**, 6205 (2015).
[29]C. J. Wan, J. M. Zhou, Y. Shi, and Q. Wan, IEEE Electron Device Lett. **35**, 414 (2014).
[30]J. C. Phillips, Rep. Prog. Phys. **59**, 1133 (1996).
[31]H. Scher, M. F. Shlesinger, and J. T. Bendler, Phys. Today **44**(1), 26 (1991).
[32]J. Kakalios, R. A. Street, and W. B. Jackson, Phys. Rev. Lett. **59**, 1037 (1987).
[33]K. Kremer and G. S. Grest, J. Chem. Phys. **92**, 5057 (1990).
[34]M. J. Panzer and C. D. Frisbie, Adv. Funct. Mater. **16**, 1051 (2006).
[35]S. M. Sze and K. K. Ng, *Physics of Semiconductor Devices*, 3 ed. (Wiley-Interscience, 2006).
[36]J. C. Lopez, Nat. Rev. Neurosci. **2**, 307 (2001).
[37]K. M. MacLeod, Hear. Res. **279**, 13 (2011).
[38]S. G. Hu, Y. Liu, T. P. Chen, Z. Liu, Q. Yu, L. J. Deng, Y. Yin, and S. Hosaka, Appl. Phys. Lett. **102**, 183510 (2013).